CHINESE OPTICS LETTERS

Vol. 21, No. 12 | December 2023

All-fiber laser amplification at 1948 nm based on double-cladding Tm/Al co-doped photonic crystal fiber fabricated by laser additive manufacturing

Yongwei Shi (史勇伟)[1,2,3], Nan Zhao (赵 楠)[1,2,3*], Jiantao Liu (刘建涛)[2,3], Jiaming Li (李嘉铭)[2,3,4], Zhiyun Hou (侯峙云)[2,3], and Guiyao Zhou (周桂耀)[2,3]

[1] School of Electronics and Information, Guangdong Polytechnic Normal University, Guangzhou 510665, China

[2] Guangdong Provincial Key Laboratory of Nanophotonic Functional Materials and Devices, South China Normal University, Guangzhou 510006, China

[3] Guangzhou Key Laboratory for Special Fiber Photonic Devices, South China Normal University, Guangzhou 510006, China

[4] Guangdong Provincial Key Laboratory of Industrial Ultrashort Pulse Laser Technology, Shenzhen 518055, China

*Corresponding author: zhaonan@gpnu.edu.cn

Received June 25, 2023 | Accepted July 14, 2023 | Posted Online December 11, 2023

In this work, we demonstrated the double-cladding Tm/Al co-doped photonic crystal fiber (PCF) by laser additive manufacturing. The measurements show that the fiber was heavily doped with a Tm^{3+} concentration of 2.13% (mass fraction) without any crystallization. The splicing property of PCF was studied, and the integrity of the PCF air holes was maintained during the splicing process. The PCF with combiner pigtail has a splice loss of 0.23 dB. The all-fiber Tm/Al co-doped PCF amplifier system achieves a slope efficiency of 13% at 1948 nm with an output laser power of nearly 1.59 W. An upconversion process was also observed under laser excitation with a 1064 nm pulse. This method provides a new idea to deal with Tm-doped PCF fabrication and promotes the promising application of 2 μm fiber lasers.

Keywords: photonic crystal fiber; laser; laser amplification.
DOI: 10.3788/COL202321.121401

1. Introduction

Rare-earth elements as doped materials in lasers have been developed for years, of which thulium (Tm)-doped lasers, emitting light in the mid-infrared 2.0 μm band, have become a hot spot in current research due to their unique advantages in ophthalmic medical treatment[1], atmospheric communication[2], and the military field[3]. A photonic crystal fiber (PCF) provides the characteristics of endless single mode, adjustable dispersion, and high nonlinearity. The main advantage of PCF in the application of fiber amplifiers and fiber lasers is that it can flexibly design the fine performance of double-cladding PCF[4]. Through the air hole, the outer cladding index of double-cladding PCF can approach one, thereby adding the NA of inner and outer cladding to improve the coupling efficiency of the pump laser. It also has the advantage of ensuring the signal light works with the signal mode at a large core diameter, and it not only separates the core fiber heart from the high-power laser but also keeps good beam quality. Meanwhile, a high doping concentration is required for achieving 200% quantum efficiency of cross-relaxation (CR)[5]. The flexible design advantages of PCFs can be well used in Tm-doped fibers[6]. In the ultrafast optical region, Gaida *et al.* achieved a pulse peak power of more than 4 MW at sub-700 fs pulse duration by Tm-doped PCF[7]. In 2020, Lee *et al.* attained a linearly-polarized amplifier with 1.5 ns, 100 kHz pulse train, and up to 250 μJ pulse energy[8]. In addition to these, many new reports about ultrafast optics will probably be optimized using PCF in the future[9–13]. In the CW laser region, Jansen *et al.* fabricated the large-area mode Tm-doped PCF and applied it to the laser. It finally got more than 52 W of output and 32.5% slope efficiency[4]. In 2013, Gaida *et al.* applied Tm-doped PCF rods and achieved 4 W seed output power at 1960 nm; the slope efficiency was 20.1%[14]. In 2016, Molardi *et al.* designed the Tm-doped PCF with a core diameter of ~80 μm and a hole size to pitch ratio d/Λ of 0.2. The finite-element method simulated the single-mode operation and gained a ratio value of 0.54 between the fundamental mode and the high-order mode[15]. In 2022, Kang *et al.* prepared Tm/Ho co-doped lanthanum aluminosilicate PCF and presented strong broadband luminescence characteristics[16]. Furthermore, various fabrication methods have been applied to get a large mode area and high-doping core materials[17–20]. In 2019, Chen *et al.* fabricated the Tm/Al co-doped PCF by the laser sintering technique to get 740 mW output power at 1.95 μm and a slope efficiency of 16.73%[21]. In

2020, Liu *et al.* used laser additive manufacturing technology to produce Tm/Al co-doped 2 μm PCF and obtained a slope efficiency of 13.9%[22]. However, space structure was generally applied in the above research work due to the splicing difficulty of PCF, which is not conducive to the integration of fiber lasers. The doping homogeneity and concentration also need to be improved for the promising application of Tm-doped PCFs.

In this work, we fabricated a heavily Tm/Al co-doped PCF by laser additive manufacturing, and the laser properties in an all-fiber experiment were conducted. The splicing loss between the PCF and double-cladding passive fiber was discussed. The upconversion process of Tm-doped PCF under 1064 nm pulse laser excitation was also performed. This work helps to promote the applications of Tm-doped PCF around eye-safe as well as visible wavelength ranges.

2. Experiment

The Tm-doped PCF was fabricated by our self-developed laser additive manufacturing[22] and drawn to fiber through a stack-and-draw technique. Figure 1 shows the detail of the laser additive manufacturing process, i.e., the silica rod is fused using output energy from the CO_2 laser, then Tm is added to obtain the Tm-doped rod, and the PCF is drawn after polishing.

The fiber profile and doping concentration were measured by electron probe microanalysis (EPMA) and are shown in Fig. 2. The double-cladding Tm/Al co-doped PCF has a good microstructure periodic arrangement. The diameters of the fiber core, inner cladding, outer cladding, and bare fiber were measured at 40, 200, 250, and 400 μm, respectively. The hole size to pitch ratio (d/Λ) was 0.1 for inner cladding, corresponding to a 13 μm pitch value. The concentrations of the Tm element in the PCF core in Fig. 2(b) have relatively good uniformity and no obvious cluster. The measured doping concentrations of Tm^{3+} and Al^{3+} were 2.13% and 1.77% (mass fractions), respectively. Figure 2(c) is the result of the line scanning of PCF. Tm and Al are roughly evenly distributed in the fiber core under their respective orders of magnitude.

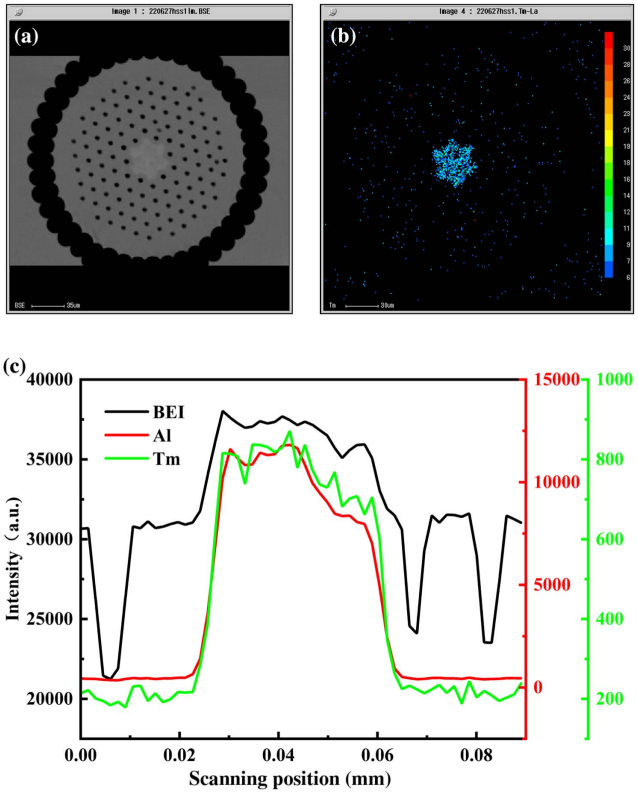

Fig. 2. (a) Electron microscope image of Tm/Al co-doped silica fiber; (b) EPMA mapping of the Tm elements in the core; (c) linear analysis of the PCF core.

A master-oscillator-power-amplifier (MOPA) system was established to measure the fiber laser properties, as shown in Fig. 3. The seed source was a 1948 nm self-built laser that can provide 4 W output power, and the 793 nm remaining pump light was removed through a cladding power stripper (CPS). A $(2+1)\times 1$ combiner was used to couple the seed source and 793 nm pump power through the signal and pump arm, respectively. Afterward, the double-cladding Tm/Al co-doped PCF was spliced to the combiner pigtail by LZM-100 to amplify the seed source power. At the end of the PCF, the laser beam was collimated by a lens. Then, the residual 793 nm pump light was filtered by a long-pass filter behind the lens. Finally, the spectrum and the power level were measured by an optical spectrum analyzer (OSA) and optical power meter, respectively.

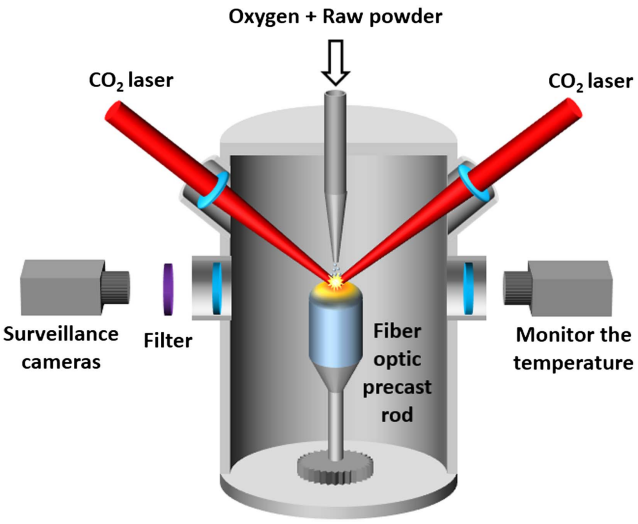

Fig. 1. Experiment of laser additive manufacturing.

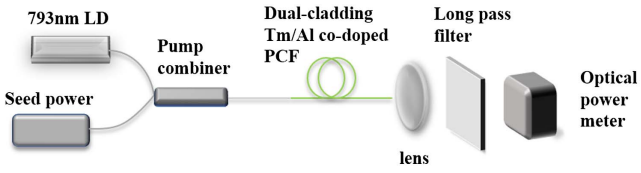

Fig. 3. Single-stage MOPA system of double-cladding Tm/Al co-doped PCF at 1948 nm.

3. Analysis of Results

In the PCF cutting process, the wavefront of the oscillating wave forms a circle, with the knife edge as the center of the circle[23]. Since the air holes are tightly arranged rings that prevent the propagation of oscillating waves, a suitable tension force choice is important. The uneven end face of the fiber cut is shown in Fig. 4(a). The fiber will not break under weak tension force, while too much tension force will cause a time difference when the inner and outer claddings of the fiber break, resulting in a different tension force and an uneven end face. For our fabricated Tm-doped PCF, the cutting parameters were optimized to be 470 gN of cut tension and 2700 gN of left and right clamping force. A smooth fiber end was obtained, as shown in Fig. 4(b), facilitating subsequent splicing operations.

A CO_2 laser (Fujikura LZM-100) was utilized to splice the double-cladding Tm/Al co-doped PCF with the combiner output pigtail[24], which has a visible advantage in dealing with air-hole collapse. When the heating temperature of the fiber end is higher than its softening temperature, the surface tension of the material will exceed the viscosity, causing the pores to collapse rapidly during the splicing process. Figure 5(a) shows the air hole force images when the PCF is heated. The point P on the outside of the hole was mainly forced by the surface tension F_p, the gravity F_g, and the pressure F_σ formed by the difference in pressure inside and outside the hole. During the splicing process, the PCF air hole communicates with the atmosphere, and F_σ can be regarded as zero. During force analysis, only gravity and surface tension are considered. The force analysis of the P point is shown in Eq. (1),

$$F_x = \sigma\left(\frac{1}{R}+\frac{1}{r}\right) r \sin\theta \mathrm{d}z\mathrm{d}\varphi, \tag{1}$$

$$F_y = \left[\rho g(R-y) + \rho\left(\frac{1}{R}+\frac{1}{r}\right)\cos\theta\right]\mathrm{d}z\mathrm{d}\varphi, \tag{2}$$

where σ is surface tension, ρ is the density of the fiber medium, g is the acceleration of gravity, and R and r are the radius of the fiber and the air-hole radius, respectively.

The deformation distances of the P point at the x axis and y axis can be expressed by S_x and S_y,

$$\frac{\partial^2 S_x}{\partial t^2} = \frac{F_x}{\eta m}, \tag{3}$$

$$\frac{\partial^2 S_y}{\partial t^2} = \frac{F_y}{\eta m}, \tag{4}$$

where η is the adhesion coefficient of fiber, and m is mass.

According to the start condition, $S_x = 0$, $S_y = 0$, and $t = 0$, the deformation distance of the air hole is as follows:

$$S = \frac{\sqrt{F_x^2 + F_y^2}}{\eta m} t^2, \tag{5}$$

where t is the melt time of the PCF. The viscosity factor and the tension factor can be explained by the molecular dynamics theory,

$$\eta = \frac{h\rho N_A}{M} \exp\left(\frac{E_0}{RT}\right), \tag{6}$$

$$\sigma = \frac{0.3}{N_A^{\frac{1}{3}}}\left(\frac{\rho}{M}\right)^{2/3}, \tag{7}$$

where M is the molecular number of fiber medium, E_0 is the activation energy of optical fiber medium; h, N_A, and R are the Planck constant, the Avogadro constant, and the molar gas constant, respectively.

From Eqs. (6) and (7), we can see that σ is insensitive to temperature, and η will decline when the temperature increases, resulting in the air-hole collapse. The validation of collapse is shown by Eq. (8),

$$V_{\text{collapse}} = \frac{\sigma}{\eta}. \tag{8}$$

Equation (8) shows that V_{collapse} was related to η; the higher the temperature, the faster V_{collapse} drops, and the faster the air holes collapse. The PCF air hole has collapsed under the high temperature in Fig. 5(b). For reliable splicing quality, the final cut end face angle should be less than 1°. To avoid the collapse

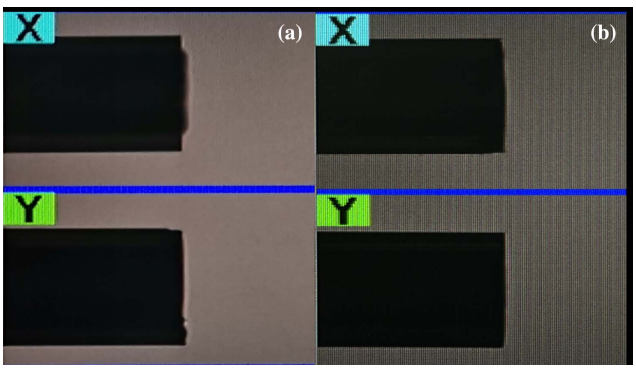

Fig. 4. (a) The end faces cut is uneven; (b) the end faces cut is smooth.

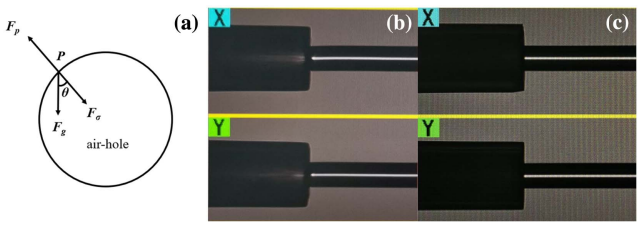

Fig. 5. (a) PCF air-hole force map; (b) the picture of collapsed air hole; (c) acceptability results of splice PCF with passive fiber.

of the PCF air hole caused by heating under high temperature, the power of the CO_2 laser is controlled to be 18 W and the discharge duration is 1200 ms, which can minimize the air-hole collapse and make the splice effect reach the ideal degree. If the core diameter is not equal, the transverse tension will make the splice point fracture, but it can withstand longitudinal tensile. The quality of the weld is independent of its ability to withstand lateral tensile forces.

The PCF with combiner pigtails has a splice loss of 0.23 dB. Losses due to mode-field mismatch are also introduced when the PCF and the pigtail are concatenated under the condition that the core diameters are perfectly aligned; that is, intrinsic losses are neglected, and the PCF air holes do not collapse[25].

Figure 6 is the near-Gaussian shape beam profile of the PCF fiber amplifier, where a slightly irregular beam was observed due to multiple transverse modes. Another reason may be the mode mismatch: the seed source splice with PCF has a light leakage absorbed by cladding. The splice quality is an important factor in the amplifier system, and it will be improved in our next work.

Figure 7(a) shows the laser spectra measured by MAYA2000 Pro (200 to 1100 nm) and NIR Quest 256 (900 to 2500 nm). The spectral intensity at 1948 nm was enhanced with the pump power increasing. Figure 7(b) is the MOPA system amplifier slope efficiency. At 0.56 W seed input power, about 1 W of power amplification was achieved. Finally, 1.59 W laser output power at 1948 nm was obtained, corresponding to 13% of slope efficiency. The output laser power was linearly enhanced, and further increase was limited by the available pump power. The low slope efficiency might be attributed to the doping fluctuation, and higher doping concentration is expected to help improve efficiency.

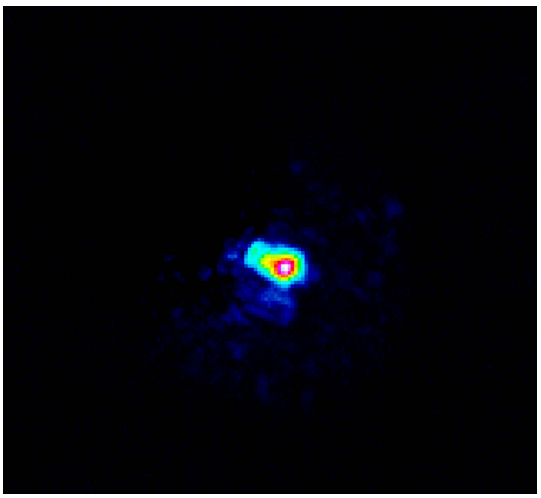

Fig. 6. Measured profile of MOPA system output beam.

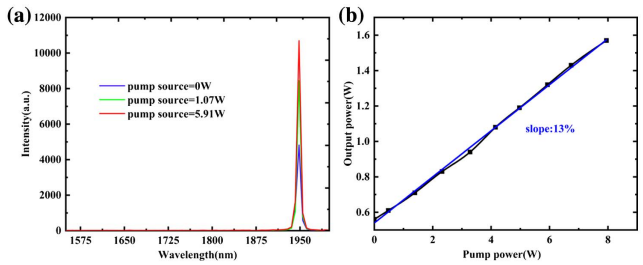

Fig. 7. (a) Spectra of seed source and pump source at different powers; (b) slope efficiency of double-cladding Tm/Al co-doped PCF amplifier.

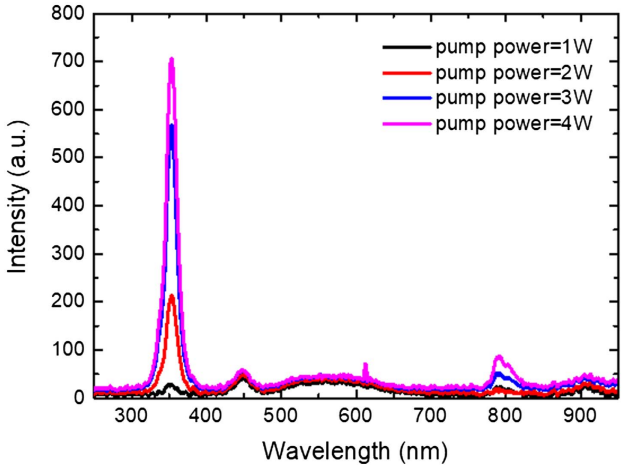

Fig. 8. Upconversion emission spectra under 1064 nm laser excitation.

Figure 8 shows the upconversion emission spectra of the double-cladding Tm/Al co-doped PCF under different power of 1064 nm fiber laser excitation. The pump source has an average power of 4 W, corresponding to 160 ps pulse duration, 1 MHz repetition frequency, and 25 kW peak power. Emission bands centered at 360, 456, 660, and 800 nm were observed, which was attributed to transitions of $^1D_2$–$^3H_6$ (353 nm), $^1D_2$–$^3F_4$ (450 nm), $^1G_4$–$^3F_4$ (620 nm), and $^3H_4$–$^3H_6$ (792 nm), respectively. As the pump intensity increases to a high excitation intensity, such as 6000 W/cm^2, four emission bands take place almost simultaneously. In our prepared glass, the 353 nm upconversion process is stronger than the other three bands, which might be caused by the intrinsic bi-stability characteristics of the level population concentration of the Tm^{3+} system[26]. This indicates the potential application in the ultraviolet region.

4. Conclusion

In this work, we present a double-cladding Tm/Al co-doped PCF fabricated by laser additive manufacturing and its all-fiber laser amplifier. A smooth cut end and low splicing loss (0.23 dB) of our Tm-doped PCF were achieved, providing an experimental basis for power amplification. Finally, a slope efficiency of 13% with 1.59 W laser power was obtained. In addition, the upconversion emission indicates the possibility of applying the double-cladding Tm/Al co-doped PCF to short-wavelength applications. Applying the all-fiber structure of Tm-doped PCF lays the foundation for the all-fiber application and integration of PCFs. The above results indicate that the laser amplification potential of the double-cladding Tm/Al co-doped PCF at

1948 nm is yet to be developed and that it also has great advantages in the short-wavelength direction, which will be greatly exploited in the future in the field of fiber lasers.

Acknowledgement

This work was supported by the National Natural Science Foundation of China (Nos. 61735005, 62105105, and 62005081), the Guangdong Basic and Applied Basic Research Foundation (Nos. 2020A1515110985 and 2021A1515011932), the Young Talent Support Project of Guangzhou Association for Science and Technology (No. QT-2023-007), and the Science and Technology Project of Henan Science and Technology Department (No. 232102220014).

References

1. S. J. Xia, "Two-micron (thulium) laser resection of the prostate-tangerine technique: a new method for BPH treatment," Asian J. Androl. **11**, 277 (2009).
2. Z. Y. Zhang, K. T. V. Grattan, A. W. Palmer, and B. T. Meggitt, "Thulium-doped intrinsic fiber optic sensor for high temperature measurements (>1100°C)," Rev. Sci. Instrum. **69**, 3210 (1998).
3. N. M. Fried and K. E. Murray, "New technologies in endourology - high-power thulium fiber laser ablation of urinary tissues at 1.94 μm," J. Endourol. **19**, 25 (2005).
4. F. Jansen, F. Stutzki, C. Jauregui, J. Limpert, and A. Tunnermann, "High-power very large mode-area thulium-doped fiber laser," Opt. Lett. **37**, 4546 (2012).
5. S. D. Jackson, "Cross relaxation and energy transfer upconversion processes relevant to the functioning of 2 μm Tm^{3+}-doped silica fibre lasers," Opt. Commun. **230**, 197 (2004).
6. Y. S. Lee, C. G. Lee, F. Bahloul, S. Kim, and K. Oh, "Simultaneously achieving a large negative dispersion and a high birefringence over Er and Tm dual gain bands in a square lattice photonic crystal fiber," J. Lightwave Technol. **37**, 1254 (2019).
7. C. Gaida, F. Stutzki, M. Gebhardt, F. Jansen, A. Wienke, U. D. Zeitner, F. Fuchs, C. Jauregui, D. Wandt, D. Kracht, J. Limpert, and A. Tünnermann, "Sub-700 fs pulses at 152 W average power from a Tm-doped fiber CPA system," Proc. SPIE **9344**, 93441K (2015).
8. E. Lee, B. Sun, J. Luo, S. Singh, D. Choudhury, D. Yong, X. Yu, and Q. Wang, "Compact pulsed thulium-doped fiber laser for topographical patterning of hydrogels," Opto-Electron. Adv. **3**, 190039 (2020).
9. Z. Zhang, J. Zhang, Y. Chen, T. Xia, L. Wang, B. Han, F. He, Z. Sheng, and J. Zhang, "Bessel terahertz pulses from superluminal laser plasma filaments," Ultrafast Sci. **2022**, 9870325 (2022).
10. C. Zhang, J. Liu, Y. Gao, X. Li, H. Lu, Y. Wang, J. Feng, J. Lu, K. Ma, and X. Chen, "Porous nickel oxide micron polyhedral particles for high-performance ultrafast photonics," Opt. Laser Technol. **146**, 107546 (2022).
11. M. Wang, M. Liu, Y. Chen, D. Ouyang, J. Zhao, J. Pei, and S. Ruan, "Stable noise-like pulse generation in all-PM mode-locked Tm-doped fiber laser based on NOLM," Chin. Opt. Lett. **19**, 091402 (2021).
12. Z. X. Zhao, H. Chen, Z. M. Zhang, J. T. Li, F. X. Zhu, W. Wan, F. He, H. F. Wei, K. K. Chen, and P. G. Yan, "High peak power femtosecond cylindrical vector beams generation in a chirped-pulse amplification laser system," Chin. Opt. Lett. **20**, 031405 (2022).
13. Q. Hao, W. Liu, Y. Zu, Y. Wang, J. Liu, and L. Su, "Highly efficient dual-wavelength acousto-optically *Q*-switched Tm,La:CaF_2 laser," Chin. Opt. Lett. **20**, 111402 (2022).
14. C. Gaida, M. Gebhardt, P. Kadwani, L. Leick, J. Broeng, L. Shah, and M. Richardson, "Peak power scaling in Tm doped fiber lasers to MW-level," Proc. SPIE **8601**, 86012Y (2013).
15. C. Molardi, E. Coscelli, A. Cucinotta, and S. Selleri, "Thermo-optical effects in Tm-doped large mode area photonic crystal fibers," Proc. SPIE **8961**, 89612Q (2014).
16. J. Kang, Z. Mo, Z. Huang, J. Yang, W. Ma, J. Liu, C. Xia, Z. Hou, and G. Zhou, "Fabrication and optical properties of Tm^{3+}/Ho^{3+} co-doped lanthanum aluminosilicate photonic crystal fiber for 2 μm fiber lasers," J. Non-Cryst. Solids **596**, 121869 (2022).
17. J. C. Knight, T. A. Birks, P. S. J. Russell, and J. P. de Sandro, "Properties of photonic crystal fiber and the effective index model," J. Opt. Soc. Am. A **15**, 748 (1998).
18. S. Wang, Z. Li, C. Yu, M. Wang, S. Feng, Q. Zhou, D. Chen, and L. Hu, "Fabrication and laser behaviors of Yb^{3+} doped silica large mode area photonic crystal fiber prepared by sol–gel method," Opt. Mater. **35**, 1752 (2013).
19. Y. Chu, Y. Yang, X. Hu, Z. Chen, Y. Ma, Y. Liu, Y. Wang, L. Liao, Y. Xing, H. Li, J. Peng, N. Dai, J. Li, and L. Yang, "Yb^{3+} heavily doped photonic crystal fiber lasers prepared by the glass phase-separation technology," Opt. Express **25**, 24061 (2017).
20. M. Devautour, P. Roy, S. Fevrier, C. Pedrido, F. Sandoz, and V. Romano, "Nonchemical-vapor-deposition process for fabrication of highly efficient Yb-doped large core fibers," Appl. Opt. **48**, G139 (2009).
21. Y. Chen, J. Liu, N. Zhao, W. Zhang, M. Zhu, G. Zhou, and Z. Hou, "Manufacture and spectroscopic analysis of Tm^{3+}-doped silica glass and microstructure optical fiber through the laser sintering technique," Appl. Phys. Express **12**, 122012 (2019).
22. J. Liu, N. Zhao, Y. Chen, M. Zhu, J. Li, S. Rong, Z. Hou, and G. Zhou, "Tm/Al co-doped silica glass prepared by laser additive manufacturing technology for 2-μm photonic crystal fiber laser," J. Lightwave Technol. **38**, 1486 (2020).
23. https://www.thorlabs.com/images/TabImages/Application_note_-_stripping_cleaving_and_coupling.pdf.
24. L. Xiao, M. S. Demokan, W. Jin, Y. Wang, and C. L. Zhao, "Fusion splicing photonic crystal fibers and conventional single-mode fibers: microhole collapse effect," J. Lightwave Technol. **25**, 3563 (2007).
25. Y. L. Hoo, W. Jin, J. Ju, and H. L. Ho, "Loss analysis of single-mode fiber/photonic-crystal fiber splice," Microw. Opt. Technol. Lett. **40**, 378 (2004).
26. L. Li, Q. Gong, X. Zhang, L. Chen, and Y.-R. Shen, "Bistable chromatic switching in 648 nm laser pumped Tm-doped crystal," Proc. SPIE **6839**, 68390R (2007).